

Dipole moment and rovibrational intensities in the electronic ground state of NH_3 : Bridging the gap between ab initio theory and spectroscopic experiment

Sergei N. Yurchenko, Miguel Carvajal, Hai Lin, Jingjing Zheng, Walter Thiel, and Per Jensen

Citation: *J. Chem. Phys.* **122**, 104317 (2005); doi: 10.1063/1.1862620

View online: <https://doi.org/10.1063/1.1862620>

View Table of Contents: <http://aip.scitation.org/toc/jcp/122/10>

Published by the [American Institute of Physics](#)

Articles you may be interested in

[Potential-energy surface for the electronic ground state of \$\text{NH}_3\$ up to \$20000\text{cm}^{-1}\$ above equilibrium](#)

The Journal of Chemical Physics **123**, 134308 (2005); 10.1063/1.2047572

[An accurate global potential energy surface, dipole moment surface, and rovibrational frequencies for \$\text{NH}_3\$](#)

The Journal of Chemical Physics **129**, 214304 (2008); 10.1063/1.3025885

[Vibrational energies for \$\text{NH}_3\$ based on high level ab initio potential energy surfaces](#)

The Journal of Chemical Physics **117**, 11265 (2002); 10.1063/1.1521762

[A global electric dipole function of ammonia and isotopomers in the electronic ground state](#)

The Journal of Chemical Physics **119**, 10724 (2003); 10.1063/1.1617272

[A global potential energy surface and dipole moment surface for silane](#)

The Journal of Chemical Physics **143**, 244317 (2015); 10.1063/1.4938563

[Modeling the spectrum of the \$2\nu_2\$ and \$\nu_4\$ states of ammonia to experimental accuracy](#)

The Journal of Chemical Physics **145**, 124301 (2016); 10.1063/1.4961656

PHYSICS TODAY

WHITEPAPERS

ADVANCED LIGHT CURE ADHESIVES

Take a closer look at what these environmentally friendly adhesive systems can do

READ NOW

PRESENTED BY
 **MASTERBOND**
ADHESIVES | SEALANTS | COATINGS

Dipole moment and rovibrational intensities in the electronic ground state of NH₃: Bridging the gap between *ab initio* theory and spectroscopic experiment

Sergei N. Yurchenko^{a)}

Max-Planck-Institut für Kohlenforschung, Kaiser-Wilhelm-Platz 1, D-45470 Mülheim an der Ruhr, Germany

Miguel Carvajal

Departamento de Física Aplicada, Facultad de Ciencias Experimentales, Avenida de las FF.AA. s/n, Universidad de Huelva, 21071 Huelva, Spain

Hai Lin

Department of Chemistry, University of Minnesota, Minneapolis, Minnesota 55455

Jingjing Zheng and Walter Thiel^{b)}

Max-Planck-Institut für Kohlenforschung, Kaiser-Wilhelm-Platz 1, D-45470 Mülheim an der Ruhr, Germany

Per Jensen

FB C-Theoretische Chemie, Bergische Universität, D-42097 Wuppertal, Germany

(Received 22 December 2004; accepted 6 January 2005; published online 15 March 2005)

We report theoretical values for the transition moments of an extensive set of vibrational bands in the electronic ground state of ¹⁴NH₃. For selected bands, we have further made detailed simulations of the rotational structure. The calculations are carried out by means of recently developed computational procedures for describing the nuclear motion and are based on a high-level *ab initio* potential energy surface, and high-level dipole moment surfaces, for the electronic ground state of NH₃. The reported theoretical intensity values are compared to, and found to agree very well with, corresponding experimental results. It is believed that the computational method, in conjunction with high-quality *ab initio* potential energy and dipole moment surfaces, can simulate rotation-vibration spectra of XY₃ pyramidal molecules prior to observation with sufficient accuracy to facilitate the observation of these spectra. By degrading the accuracy of selected elements of the calculations, we have also investigated the influence of customary approximations on the computed intensity values. © 2005 American Institute of Physics. [DOI: 10.1063/1.1862620]

I. INTRODUCTION

Modern *ab initio* calculations of molecular potential energy surfaces, coupled with high-level treatments of the nuclear motion, provide very accurate descriptions of the properties of isolated molecules. In particular, the theoretical calculations often yield molecular energy levels in very good agreement with the results of spectroscopic experiments. One could think that owing to the progress in theoretical methods, the assignment of molecular spectra would become increasingly trivial: The spectrum, or at least the transition frequencies, can be predicted from first principles with sufficient accuracy that the assignment of each individual transition can be straightforwardly obtained from the theoretical calculation. There are examples, such as the water molecule,^{1,2} where such a “first-principles assignment” can be made, but present-day assignment of spectra is still largely based on the more traditional methods of general pattern recognition, search for combination differences, and the least-squares fitting of the frequencies for the assigned tran-

sitions, with subsequent prediction of the frequencies for unassigned lines, by means of models involving effective rotation-vibration parameters (see, for example, Ref. 3).

In recent papers^{4–8} we have described the development and application of a theoretical model for simulating rotation-vibration spectra for isolated electronic states of XY₃ pyramidal molecules. The applications, so far, have been to the NH₃ (Refs. 4, 6, and 8) and PH₃ (Refs. 5 and 7) molecules. Initially,^{4,6} we developed a computational procedure for calculating rotation-vibration energies and wave functions of XY₃ molecules from an *ab initio* potential energy surface. With energies for ¹⁴NH₃, obtained with this procedure from a high-quality *ab initio* potential energy surface,^{4,9} we were able to assist the assignment of high-resolution molecular spectra, in that we could verify—for the most part—the tentative assignment to the $4\nu_2^+$ band¹⁰ of 55 weak transitions observed in an experimental study of the ν_1 , ν_3 , and $2\nu_4$ bands of ¹⁴NH₃.

Our theoretical model for the rotation and vibration of an XY₃ molecule (for details, see Ref. 6) is a variational (i.e., perturbation-theory-free) implementation of the Hougen–Bunker–Johns (henceforth HBJ) approach.^{11,12} The HBJ approach is designed to provide maximum separation of the rotational and vibrational motions in the quantum-

^{a)}Author to whom correspondence should be addressed. Electronic mail: yurchenko@mpi-muelheim.mpg.de

^{b)}Author to whom correspondence should be addressed. Electronic mail: thiel@mpi-muelheim.mpg.de

mechanical description, and so our model is particularly suitable for calculating the energies and wave functions of highly excited rotational states. So, recently⁷ we could generate energies and wave functions for states with $J \leq 80$ in the vibrational ground state of PH_3 and study the formation of sixfold clusters of rotational energies; these clusters are analogous to the fourfold clusters extensively discussed for XH_2 molecules (see Refs. 12 and 13 and references therein).

Since we can treat highly excited rotational states of XY_3 molecules, we can generate the energies and wave functions necessary to simulate realistic rotation-vibration spectra of them. Such simulations obviously help “bridging the gap” between *ab initio* theory and experimental spectroscopy; they are a prerequisite for the first-principles assignments mentioned above. We have already described⁸ the extension of our theoretical model to the computation of line strengths (see below) and intensities for electric dipole transitions within an isolated electronic state of an XY_3 pyramidal molecule. We have also reported⁸ the calculation of *ab initio* dipole moment surfaces for the electronic ground state of $^{14}\text{NH}_3$ together with initial applications of the new intensity model to $^{14}\text{NH}_3$ rotation-vibration transitions; in the present work we extend these calculations and, by comparing our computed intensities with the results of more approximate treatments, we make a critical assessment of various approximations customarily made in intensity calculations. For a detailed discussion of the theoretical description of the molecular rotation-vibration motion and the intensities of the associated transitions, the reader is referred to Refs. 6 and 8, respectively. The present work gives only a brief outline of the theory, intended to provide the reader with sufficient information for understanding the origin of the results that we present.

One purpose of the present paper is to determine the degree of agreement with experiment that can be obtained in “pure” *ab initio* calculations of molecular intensities. In consequence, our calculations are based on a potential energy surface and dipole moment surfaces obtained directly from *ab initio* calculations: We have made no adjustments to fit experimental data for NH_3 .

II. THE MOLECULAR DIPOLE MOMENT

A. The *ab initio* calculation

As discussed in Ref. 8, the *ab initio* dipole moment values employed in the present work were computed with the MOLPRO2000 (Refs. 14 and 15) package at the CCSD(T)/aug-cc-pVTZ level of theory (i.e., coupled cluster theory with all single and double substitutions¹⁶ and a perturbative treatment of connected triple excitations^{17,18} with the augmented correlation-consistent triple ζ basis^{19,20}) in the frozen-core approximation (abbreviated as ATZfc level). Dipole moments were computed in a numerical finite-difference procedure with an added external dipole field of 0.005 a.u. The convergence thresholds were 10^{-10} for density and 10^{-7} a.u. for energy in Hartree–Fock calculations, and 10^{-10} a.u. for energy and 10^{-10} for coefficients in CCSD(T) computations.

The *ab initio* dipole moment surface used in the present study has been determined on a six-dimensional grid (the

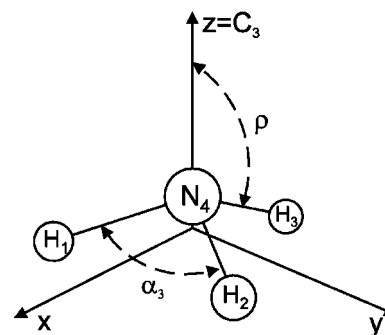


FIG. 1. The labeling of the nuclei, the molecule-fixed axis system xyz , and selected coordinates employed for NH_3 (see text).

6D-1 grid in Ref. 4) consisting of 14 400 unique geometries that form a regular grid in the range $0.85 \text{ \AA} \leq r_1 \leq r_2 \leq r_3 \leq 1.20 \text{ \AA}$ and $80^\circ \leq \alpha_1 \leq \alpha_2 \leq \alpha_3 \leq 120^\circ$. Here, r_i is the instantaneous value of the internuclear distance $\text{N}-\text{H}_i$, $i = 1, 2, 3$, and the bond angles are given as $\alpha_1 = \angle(\text{H}_2\text{NH}_3)$, $\alpha_2 = \angle(\text{H}_1\text{NH}_3)$, and $\alpha_3 = \angle(\text{H}_1\text{NH}_2)$ [see Fig. 1].

In the *ab initio* calculations the components of the molecular dipole moment are given in a right-handed Cartesian axis system $x'y'z'$ with origin in the nitrogen nucleus. The H_1 nucleus lies on the z' axis with a positive value of the z' coordinate, and the $y'z'$ plane is defined by the nitrogen nucleus and the protons H_1 and H_2 .

B. A general analytical representation of the dipole moment

In the so-called molecular bond (MB) representation,^{8,21,22} the electronically averaged dipole moment vector^{8,12} $\bar{\boldsymbol{\mu}}$ for NH_3 is given by

$$\bar{\boldsymbol{\mu}} = \bar{\mu}_1^{\text{Bond}} \mathbf{e}_1 + \bar{\mu}_2^{\text{Bond}} \mathbf{e}_2 + \bar{\mu}_3^{\text{Bond}} \mathbf{e}_3, \quad (1)$$

where the three functions $\bar{\mu}_i^{\text{Bond}}$, $i = 1, 2, 3$, depend on the vibrational coordinates, and \mathbf{e}_i is the unit vector along the $\text{N}-\text{H}_i$ bond,

$$\mathbf{e}_i = \frac{\mathbf{r}_i - \mathbf{r}_4}{|\mathbf{r}_i - \mathbf{r}_4|} \quad (2)$$

with \mathbf{r}_i as the position vector of nucleus i (the protons are labeled 1, 2, 3, and the nitrogen nucleus is labeled 4, see Fig. 1) in the axis system $x'y'z'$ defined above. As discussed in Ref. 8, the representation of $\bar{\boldsymbol{\mu}}$ in Eq. (1) is “body fixed” in the sense that it relates the dipole moment vector directly to the instantaneous positions of the nuclei (i.e., to the vectors \mathbf{r}_i). In consequence, we can use Eq. (1) to obtain the coordinates of $\bar{\boldsymbol{\mu}}$ in any axis system.

Our implementation of the MB representation for the electronic-ground-state dipole moment of NH_3 is detailed in Ref. 8; here we give only a brief outline. We express the three functions $\bar{\mu}_i^{\text{Bond}}$, $i = 1, 2, 3$, as

$$\bar{\mu}_i^{\text{Bond}} = \sum_{j=1}^3 (\mathbf{A}^{-1})_{ij} (\bar{\boldsymbol{\mu}} \cdot \mathbf{e}_j), \quad (3)$$

where $(\mathbf{A}^{-1})_{ij}$ is an element of the nonorthogonal 3×3 matrix \mathbf{A}^{-1} obtained as the inverse of

$$\mathbf{A} = \begin{pmatrix} 1 & \cos \alpha_3 & \cos \alpha_2 \\ \cos \alpha_3 & 1 & \cos \alpha_1 \\ \cos \alpha_2 & \cos \alpha_1 & 1 \end{pmatrix}. \quad (4)$$

When the molecule is planar, i.e., when $\alpha_1 + \alpha_2 + \alpha_3 = 2\pi$, the determinant $|\mathbf{A}| = 0$ and \mathbf{A} cannot be inverted. For planar geometries \mathbf{e}_1 , \mathbf{e}_2 , and \mathbf{e}_3 are linearly dependent and there are infinitely many possible values of $(\bar{\mu}_1^{\text{Bond}}, \bar{\mu}_2^{\text{Bond}}, \bar{\mu}_3^{\text{Bond}})$. In this case we set $\bar{\mu}_3^{\text{Bond}} = 0$ in Eq. (1) and express $\bar{\boldsymbol{\mu}}$ in terms of \mathbf{e}_1 and \mathbf{e}_2 only, i.e., we determine $\bar{\mu}_1^{\text{Bond}}$ and $\bar{\mu}_2^{\text{Bond}}$ in terms of $\bar{\boldsymbol{\mu}} \cdot \mathbf{e}_1$ and $\bar{\boldsymbol{\mu}} \cdot \mathbf{e}_2$.

We have shown in Ref. 8 that the projections $\bar{\boldsymbol{\mu}} \cdot \mathbf{e}_j$, $j = 1, 2, 3$, in Eq. (3) can be expressed in terms of the geometrically defined coordinates $r_1, r_2, r_3, \alpha_1, \alpha_2$, and α_3 . By utilizing that a permutation of the protons in NH₃ does not change the molecular dipole moment¹² we further derived⁸ that all three projections are given in terms of a single function $\bar{\mu}_0(r_1, r_2, r_3, \alpha_1, \alpha_2, \alpha_3)$:

$$\bar{\boldsymbol{\mu}} \cdot \mathbf{e}_1 = \bar{\mu}_0(r_1, r_2, r_3, \alpha_1, \alpha_2, \alpha_3) = \bar{\mu}_0(r_1, r_3, r_2, \alpha_1, \alpha_3, \alpha_2), \quad (5)$$

$$\bar{\boldsymbol{\mu}} \cdot \mathbf{e}_2 = \bar{\mu}_0(r_2, r_3, r_1, \alpha_2, \alpha_3, \alpha_1) = \bar{\mu}_0(r_2, r_1, r_3, \alpha_2, \alpha_1, \alpha_3), \quad (6)$$

$$\bar{\boldsymbol{\mu}} \cdot \mathbf{e}_3 = \bar{\mu}_0(r_3, r_1, r_2, \alpha_3, \alpha_1, \alpha_2) = \bar{\mu}_0(r_3, r_2, r_1, \alpha_3, \alpha_2, \alpha_1). \quad (7)$$

This function is expressed as an expansion

$$\begin{aligned} \bar{\mu}_0 = & \sum_k \mu_k^{(0)} \xi_k + \sum_{k,l} \mu_{k,l}^{(0)} \xi_k \xi_l + \sum_{k,l,m} \mu_{k,l,m}^{(0)} \xi_k \xi_l \xi_m \\ & + \sum_{k,l,m,n} \mu_{k,l,m,n}^{(0)} \xi_k \xi_l \xi_m \xi_n + \dots, \end{aligned} \quad (8)$$

in the variables

$$\xi_k = r_k \exp(-\beta^2 r_k^2), \quad k = 1, 2, 3, \quad (9)$$

$$\xi_l = \cos(\alpha_{l-3}) - \cos\left(\frac{2\pi}{3}\right) = \frac{1}{2} + \cos(\alpha_{l-3}), \quad l = 4, 5, 6, \quad (10)$$

which are chosen such that $\bar{\mu}_0 = 0$ for $(r_1 = r_2 = r_3 = 0, \alpha_1 = \alpha_2 = \alpha_3 = 2\pi/3)$. Following Marquardt *et al.*,²² we have introduced the factor $\exp(-\beta^2 r_k^2)$ in order to keep the expansion in Eq. (8) from diverging at large r_i .

The function $\bar{\mu}_0(r_1, r_2, r_3, \alpha_1, \alpha_2, \alpha_3)$ is invariant to the simultaneous interchanges $r_2 \leftrightarrow r_3$ and $\alpha_2 \leftrightarrow \alpha_3$ [Eq. (5)] and, therefore, the expansion coefficients $\mu_k^{(0)}$, $\mu_{k,l}^{(0)}$, $\mu_{k,l,m}^{(0)}$ and $\mu_{k,l,m,n}^{(0)}$ in Eq. (8) are subject to constraints. In general, we have

$$\mu_{k',l',m',\dots}^{(0)} = \mu_{k,l,m,\dots}^{(0)} \quad (11)$$

if the indices k', l', m', \dots are obtained from k, l, m, \dots by replacing all indices 2 by 3, all indices 3 by 2, all indices 5 by 6, and all indices 6 by 5. For instance, $\mu_2^{(0)} = \mu_3^{(0)}$, $\mu_5^{(0)} = \mu_6^{(0)}$, $\mu_{2,2}^{(0)} = \mu_{3,3}^{(0)}$, $\mu_{5,5}^{(0)} = \mu_{6,6}^{(0)}$, $\mu_{1,2,2}^{(0)} = \mu_{1,3,3}^{(0)}$, and $\mu_{1,2,6}^{(0)} = \mu_{1,3,5}^{(0)}$.

We have determined the values of the expansion parameters in Eq. (8), which we take to fourth order, in a least-squares fitting to the $3 \times 14\,440$ *ab initio* dipole moment projections $\bar{\boldsymbol{\mu}} \cdot \mathbf{e}_j$, $j = 1, 2, 3$, calculated *ab initio* for NH₃ at the CCSD(T)/aug-cc-pVTZ level of theory (Sec. II A). Details of this fitting are given in Ref. 8. We could usefully vary 91 parameters in the final fitting, which had a root-mean-square (rms) deviation of 0.0006 D. Table I lists the optimized parameter values. Parameters, whose absolute values were determined to be less than their standard errors in initial fittings, were constrained to zero in the final fitting and omitted from the table. Furthermore, we give in the table only one member of each parameter pair related by Eq. (11).

As already reported,⁴ the ATZfc dipole moment surface gives rise to an “equilibrium” moment of $\mu_e = 1.5198$ D at the ATZfc *ab initio* equilibrium geometry of $r_1 = r_2 = r_3 = r_e = 1.0149$ Å and $\alpha_1 = \alpha_2 = \alpha_3 = \alpha_e = 106.4^\circ$. The experimental value²³ for μ_e is (1.561 ± 0.005) D.

III. COMPUTATIONAL DETAILS

A. Rotation-vibration wave functions

We wish to calculate the intensities of electric dipole transitions within the ground electronic state of NH₃. We consider a transition from an initial state i with rotation-vibration wave function $|\Phi_{\text{rv}}^{(i)}\rangle$ to a final state f with rotation-vibration wave function $|\Phi_{\text{rv}}^{(f)}\rangle$. As discussed at length in Ref. 6, the rotation-vibration wave functions $|\Phi_{\text{rv}}^{(i)}\rangle$ and $|\Phi_{\text{rv}}^{(f)}\rangle$ are obtained, together with the associated rotation-vibration energies, in variational calculations, i.e., by diagonalization of a matrix representation of the rovibrational Hamiltonian. Consequently, the wave functions are expressed as linear combinations of basis functions [see Eq. (65) of Ref. 6]:

$$|\Phi_{\text{rv}}^{(w)}\rangle = \sum_{VK\tau_{\text{rot}}} C_{VK\tau_{\text{rot}}}^{(w)} |J_w K m_w \tau_{\text{rot}}\rangle |V\rangle, \quad w = i \text{ or } f, \quad (12)$$

where $C_{VK\tau_{\text{rot}}}^{(w)}$ are expansion coefficients, $|J_w K m_w \tau_{\text{rot}}\rangle$ is a symmetrized rotational basis function, and the vibrational basis function $|V\rangle$ is given by

$$|V\rangle = |n_1\rangle |n_2\rangle |n_3\rangle |n_b, l_b, \tau_{\text{bend}}\rangle |n_i, J_w, K, \tau_{\text{inv}}\rangle. \quad (13)$$

All the functions $|n_1\rangle$, $|n_2\rangle$, $|n_3\rangle$, $|n_b, l_b, \tau_{\text{bend}}\rangle$, and $|n_i, J_w, K, \tau_{\text{inv}}\rangle$, and the quantum numbers labeling them are defined in detail in Ref. 6: $|n_1\rangle$, $|n_2\rangle$, and $|n_3\rangle$ are one-dimensional Morse-oscillator eigenfunctions describing the stretching motion of the XY₃ molecule, $|n_b, l_b, \tau_{\text{bend}}\rangle$ is a symmetrized eigenfunction of the two-dimensional harmonic oscillator modeling the small-amplitude bending motion, and $|n_i, J_w, K, \tau_{\text{inv}}\rangle$ is a symmetrized inversion basis function obtained by numerical solution of a zero-order inversion Schrödinger equation. All three quantum numbers τ_{rot} , τ_{bend} , and τ_{inv} assume values of 0 or 1 in such a way that the parity^{12,24} of $|J_w K m_w \tau_{\text{rot}}\rangle$ is $(-1)^{\tau_{\text{rot}}}$, the parity of $|n_b, l_b, \tau_{\text{bend}}\rangle$ is $(-1)^{\tau_{\text{bend}}}$, and the parity of $|n_i, J_w, K, \tau_{\text{inv}}\rangle$ is $(-1)^{\tau_{\text{inv}}}$.

The rotational basis functions $|J_w K m_w \tau_{\text{rot}}\rangle$ depend on three Euler angles^{6,12,24} θ, ϕ, χ , which define the orientation of the *molecule-fixed axis system* xyz relative to the space-fixed (or laboratory-fixed) axis system XYZ . The xyz axis

TABLE I. MB-representation dipole moment parameters (in D unless otherwise indicated) for the electronic ground state of NH₃.

Parameter	Value	Parameter	Value	Parameter	Value
$\beta/\text{\AA}^{-1}$	1.0928(15) ^a	$\mu_{225}^{(0)}$	-2.04(17)	$\mu_{1456}^{(0)}$	3.0190(94)
$\mu_1^{(0)}$	8.70(13)	$\mu_{226}^{(0)}$	8.95(15)	$\mu_{1466}^{(0)}$	-0.5794(93)
$\mu_3^{(0)}$	-4.632(66)	$\mu_{234}^{(0)}$	-1.961(19)	$\mu_{1566}^{(0)}$	0.5262(76)
$\mu_4^{(0)}$	0.218(11)	$\mu_{246}^{(0)}$	2.967(17)	$\mu_{1666}^{(0)}$	1.3038(73)
$\mu_5^{(0)}$	0.5155(71)	$\mu_{256}^{(0)}$	1.360(20)	$\mu_{2222}^{(0)}$	76.40(89)
$\mu_{11}^{(0)}$	-43.75(74)	$\mu_{266}^{(0)}$	3.421(22)	$\mu_{2224}^{(0)}$	7.46(17)
$\mu_{13}^{(0)}$	-4.96(25)	$\mu_{333}^{(0)}$	-73.52(94)	$\mu_{2225}^{(0)}$	6.49(20)
$\mu_{14}^{(0)}$	3.219(80)	$\mu_{334}^{(0)}$	-2.10(15)	$\mu_{2245}^{(0)}$	-3.135(20)
$\mu_{16}^{(0)}$	8.196(51)	$\mu_{344}^{(0)}$	0.4884(76)	$\mu_{2246}^{(0)}$	-1.734(26)
$\mu_{23}^{(0)}$	0.416(38)	$\mu_{444}^{(0)}$	0.3513(60)	$\mu_{2255}^{(0)}$	0.500(22)
$\mu_{33}^{(0)}$	29.71(37)	$\mu_{445}^{(0)}$	0.3849(30)	$\mu_{2256}^{(0)}$	-1.061(39)
$\mu_{34}^{(0)}$	-0.196(46)	$\mu_{466}^{(0)}$	0.4947(35)	$\mu_{2266}^{(0)}$	-2.639(35)
$\mu_{35}^{(0)}$	-5.290(45)	$\mu_{556}^{(0)}$	-0.0530(34)	$\mu_{2335}^{(0)}$	3.76(18)
$\mu_{36}^{(0)}$	0.554(53)	$\mu_{1111}^{(0)}$	-93.6(15)	$\mu_{2336}^{(0)}$	-2.45(17)
$\mu_{44}^{(0)}$	-0.5260(49)	$\mu_{1114}^{(0)}$	4.84(27)	$\mu_{2345}^{(0)}$	2.723(27)
$\mu_{46}^{(0)}$	-0.4327(47)	$\mu_{1115}^{(0)}$	11.91(18)	$\mu_{2356}^{(0)}$	-2.866(85)
$\mu_{55}^{(0)}$	-0.1960(38)	$\mu_{1122}^{(0)}$	9.70(59)	$\mu_{2366}^{(0)}$	-0.954(41)
$\mu_{56}^{(0)}$	0.6815(82)	$\mu_{1124}^{(0)}$	-2.62(14)	$\mu_{2444}^{(0)}$	-0.2227(69)
$\mu_{111}^{(0)}$	97.5(17)	$\mu_{1126}^{(0)}$	-1.802(45)	$\mu_{2456}^{(0)}$	-1.0261(55)
$\mu_{112}^{(0)}$	1.73(34)	$\mu_{1136}^{(0)}$	-3.64(19)	$\mu_{2466}^{(0)}$	-0.7438(86)
$\mu_{114}^{(0)}$	-5.25(25)	$\mu_{1146}^{(0)}$	3.268(36)	$\mu_{3335}^{(0)}$	-15.18(16)
$\mu_{115}^{(0)}$	-9.84(16)	$\mu_{1155}^{(0)}$	-0.995(35)	$\mu_{3445}^{(0)}$	-0.7453(56)
$\mu_{123}^{(0)}$	1.707(52)	$\mu_{1156}^{(0)}$	6.649(44)	$\mu_{3555}^{(0)}$	-0.6499(73)
$\mu_{124}^{(0)}$	2.40(11)	$\mu_{1222}^{(0)}$	-26.84(74)	$\mu_{3556}^{(0)}$	-0.3512(88)
$\mu_{133}^{(0)}$	12.08(70)	$\mu_{1245}^{(0)}$	2.565(41)	$\mu_{4444}^{(0)}$	-0.0903(26)
$\mu_{136}^{(0)}$	-0.69(11)	$\mu_{1256}^{(0)}$	1.120(35)	$\mu_{4445}^{(0)}$	-0.0542(14)
$\mu_{144}^{(0)}$	-0.6454(55)	$\mu_{1334}^{(0)}$	-4.64(14)	$\mu_{4466}^{(0)}$	-0.0246(13)
$\mu_{146}^{(0)}$	-4.135(22)	$\mu_{1355}^{(0)}$	3.787(34)	$\mu_{4555}^{(0)}$	-0.0704(15)
$\mu_{155}^{(0)}$	-3.868(21)	$\mu_{1366}^{(0)}$	0.518(36)	$\mu_{4556}^{(0)}$	-0.2147(13)
$\mu_{156}^{(0)}$	-6.144(27)	$\mu_{1445}^{(0)}$	0.3319(65)	$\mu_{5666}^{(0)}$	0.0617(15)
$\mu_{223}^{(0)}$	-0.794(34)	rms ^b	0.0006		

^aQuantities in parentheses are standard errors in units of the last digit given.

^bRoot-mean-square deviation of the fitting in D.

system follows the rotation of the molecule. In our HBJ-based theory, it is defined in terms of Eckart and Sayvetz conditions;^{6,12} these conditions minimize the coupling between different types of molecular motion, in particular, between rotation and vibration.

Each stretching basis function $|n_j\rangle$, $j=1,2,3$, depends on one coordinate $\Delta r_j^\ell = r_j^\ell - r_e$, where r_j^ℓ is the linearized version⁶ of the internuclear distance r_j and r_e is the equilibrium value of r_j . The bending basis function $|n_b, l_b, \tau_{\text{bend}}\rangle$ depends on the coordinates $(S_{4a}^\ell, S_{4b}^\ell)$, the linearized versions⁶ of

$$S_{4a} = \frac{1}{\sqrt{6}}(2\alpha_1 - \alpha_2 - \alpha_3), \quad (14)$$

$$S_{4b} = \frac{1}{\sqrt{2}}(\alpha_2 - \alpha_3). \quad (15)$$

Finally, the inversion basis function $|n_i, J_w, K, \tau_{\text{inv}}\rangle$ depends on the HBJ inversion coordinate^{6,25,26} ρ . In HBJ theory,¹¹ the small-amplitude vibrations [described by the coordinates $(r_1^\ell, r_2^\ell, r_3^\ell, S_{4a}^\ell, S_{4b}^\ell)$ here] are viewed as displacements from a flexible reference configuration replacing the rigid equilib-

rium structure of customary rotation-vibration theory (see, for example, Ref. 3). For the XY₃ molecules considered here, we define the reference configuration to have three equal, constant bond lengths $r_1=r_2=r_3=r_e$ and three equal but variable bond angles $\alpha_1=\alpha_2=\alpha_3$. Thus, the reference configuration has C_{3v} or D_{3h} geometrical symmetry and we define the inversion coordinate ρ as the angle between the C_3 rotational symmetry axis and any one of the N–H bonds as shown in Fig. 1. That is, $0 \leq \rho \leq \pi$ and the reference configuration is planar for $\rho = \pi/2$.

In the variational calculations the expansions of the kinetic energy factors⁶ $G_{\alpha\beta}$ and the pseudopotential⁶ U are taken to fourth order, and the potential energy V is expanded through sixth order. In the numerical integration of the inversion Schrödinger equation a grid of 1000 points is used. The size of the vibrational basis set is controlled by the parameter P_{max} where

$$P = 2(n_1 + n_2 + n_3) + n_i + n_b \leq P_{\text{max}}. \quad (16)$$

The matrices are diagonalized with routines from the LAPACK library.²⁷ Further details can be found in Ref. 6.

B. Line strengths and intensities

In the present work, we neglect hyperfine structure (i.e., the effect of the nuclear spins on the molecular energies). In this approximation, the line strength^{8,12,24} $S(f \leftarrow i)$ of the rotation-vibration transition $f \leftarrow i$ is obtained from Eq. (4) of Ref. 8:

$$S(f \leftarrow i) = g_{\text{ns}} \sum_{m_f, m_i} \sum_{A=X, Y, Z} |\langle \Phi_{\text{rv}}^{(f)} | \bar{\mu}_A | \Phi_{\text{rv}}^{(i)} \rangle|^2, \quad (17)$$

where g_{ns} is the nuclear spin statistical weight factor^{12,24} and $\bar{\mu}_A$ is the electronically averaged component of the molecular dipole moment along the space-fixed axis $A=X, Y$, or Z . The quantum numbers m_i and m_f are the projections of the total angular momentum, in units of \hbar , on the Z axis in the initial and final states, respectively.

The intensity of absorption spectra is determined by the absorption coefficient^{12,24} $\epsilon(\tilde{\nu})$ which depends on the absorption wave number $\tilde{\nu}$. If we assume the absorbing molecules to be in thermal equilibrium at an absolute temperature T , the integral of $\epsilon(\tilde{\nu})$ over an absorption line is related to the line strength as

$$I(f \leftarrow i) = \int_{\text{Line}} \epsilon(\tilde{\nu}) d\tilde{\nu} = \frac{8\pi^3 N_A \tilde{\nu}_{if} e^{-E_i/kT}}{(4\pi\epsilon_0) 3hc Q} \times [1 - \exp(-hc\tilde{\nu}_{if}/kT)] S(f \leftarrow i). \quad (18)$$

This expression is valid for the transition from the state i with energy E_i to the state f with energy E_f , where $hc\tilde{\nu}_{if} = E_f - E_i$, N_A is the Avogadro constant, h is Planck's constant, c is the speed of light in vacuum, k is the Boltzmann constant, ϵ_0 is the permittivity of free space, and, finally, Q is the partition function defined as $Q = \sum_j g_j \exp(-E_j/kT)$, where g_j is the total degeneracy of the state with energy E_j and the sum runs over all energy levels of the molecule. Experimental values of $I(f \leftarrow i)$ are obtained by numerical integration of experimentally determined $\epsilon(\tilde{\nu})$ values.

A detailed expression for the line strength of an individual rotation-vibration transition within an isolated electronic state of an XY₃ pyramidal molecule is given in Eq. (21) of Ref. 8. This expression is used in the intensity calculations reported in the present work. It is obtained by inserting Eq. (12) in Eq. (17) and expressing $\bar{\mu}_A$, $A=X, Y, Z$, in terms of $(\bar{\mu}_x, \bar{\mu}_y, \bar{\mu}_z)$, the dipole moment components along the molecule-fixed axes xyz . The line strength is expressed in terms of the vibronic matrix elements $\langle V' | \bar{\mu}_\alpha | V'' \rangle$, $\alpha=x, y, z$, and in terms of the expansion coefficients $C_{V'K'r'_{\text{rot}}}^{(f)}$ and $C_{V''K''r''_{\text{rot}}}^{(i)}$ from Eq. (12). The transformation $(\bar{\mu}_x, \bar{\mu}_y, \bar{\mu}_z) \rightarrow (\bar{\mu}_x, \bar{\mu}_y, \bar{\mu}_z)$ is carried out by means of standard techniques described, for example, in Chapter 14 of Ref. 12. Examples of the application of these techniques are given for triatomic molecules in Refs. 28 and 29.

C. The *ab initio* potential energy surface

The calculations of the present work are made with the CBS**⁻⁵ *ab initio* potential energy surface.^{4,8,9} At the first step towards determining this surface, ATZfc energies were computed for 51 816 nuclear geometries at the CCSD(T)/

aug-cc-pVTZ level of theory also used in the dipole moment calculations described in Sec. II A. At 3814 selected nuclear geometries, more accurate energies (CBS+) were determined by extrapolating the CCSD(T) results to the complete basis set limit and including corrections for relativistic effects and core-valence correlation.⁴ The differences between the ATZfc and CBS+ energies were fitted by a sixth-order polynomial in geometrically defined, internal coordinates, and the CBS**⁻⁵ surface (which is close to CBS+ quality) was generated by adding corrections, computed from the six-order polynomial, to the ATZfc energies at all 51 816 grid points. An analytical representation of this surface was obtained by fitting a sixth-order expansion, given in Eq. (57) of Ref. 4, through all CBS**⁻⁵ data points. The resulting 181 potential parameters will be published elsewhere;⁹ they are presently available from the authors on request. The CBS**⁻⁵ surface provides a complete description of the electronic-ground-state potential energy surface of NH₃ for energies up to 20 000 cm⁻¹ above equilibrium.

D. The representation of the dipole moment in the xyz axis system

In order to compute the matrix elements $\langle V' | \bar{\mu}_\alpha | V'' \rangle$ ($\alpha = x, y, z$), that enter into the expression for the line strength in Eq. (21) of Ref. 8, we must determine, from the *ab initio* results discussed in Sec. II A, the dipole moment components $(\bar{\mu}_x, \bar{\mu}_y, \bar{\mu}_z)$ in the molecule-fixed axis system xyz . As discussed extensively in Ref. 8, we aim at representing $(\bar{\mu}_x, \bar{\mu}_y, \bar{\mu}_z)$ as expansions with ρ -dependent expansion coefficients

$$\begin{aligned} \bar{\mu}_\alpha(\xi_1^\ell, \xi_2^\ell, \xi_3^\ell, \xi_{4a}^\ell, \xi_{4b}^\ell; \rho) = & \mu_0^\alpha(\rho) + \sum_k \mu_k^\alpha(\rho) \xi_k^\ell \\ & + \sum_{k \leq l} \mu_{kl}^\alpha(\rho) \xi_k^\ell \xi_l^\ell \\ & + \sum_{k \leq l \leq m} \mu_{klm}^\alpha(\rho) \xi_k^\ell \xi_l^\ell \xi_m^\ell \\ & + \sum_{k \leq l \leq m \leq n} \mu_{klmn}^\alpha(\rho) \xi_k^\ell \xi_l^\ell \xi_m^\ell \xi_n^\ell \dots \end{aligned} \quad (19)$$

in the linearized variables

$$\xi_k^\ell = 1 - \exp(-a\Delta r_k^\ell), \quad k = 1, 2, 3, \quad (20)$$

$\xi_{4a}^\ell = S_{4a}^\ell$, and $\xi_{4b}^\ell = S_{4b}^\ell$. The range parameter a occurs in the analytical representation for the potential energy function.⁶

The ρ -dependent functions $\mu_{kl\dots}^\alpha(\rho)$ ($\alpha=x$ or y) in Eq. (19) are chosen as

$$\mu_{kl\dots}^\alpha(\rho) = \sum_{s \geq 0} \mu_{kl\dots}^{\alpha(s)} (\sin \rho_0 - \sin \rho)^s, \quad 0 \leq \rho \leq \pi, \quad (21)$$

where we take $\rho_0 = \pi/2$, corresponding to the planar configuration. To represent $\bar{\mu}_z$, we choose

$$\mu_{kl\dots}^z(\rho) = \sum_{s>0} \mu_{kl\dots}^{z(s)} (\cos \rho_0 - \cos \rho)^s \quad \text{for } \frac{\pi}{2} \leq \rho \leq \pi, \quad (22)$$

and

$$\mu_{kl\dots}^z(\rho) = -\mu_{kl\dots}^z(\pi - \rho) \quad \text{for } 0 \leq \rho < \frac{\pi}{2}. \quad (23)$$

The dipole moment components $(\bar{\mu}_x, \bar{\mu}_y)$ have E' symmetry in $D_{3h}(M)$, the molecular symmetry group^{6,8,12,24} of NH_3 , and $\bar{\mu}_z$ has A_2' symmetry. The irreducible representations of $D_{3h}(M)$ are given in Table 1 of Ref. 8 and in Table A-10 of Ref. 12. The functions in Eqs. (21)–(23) are chosen so as to ensure that $(\bar{\mu}_x, \bar{\mu}_y, \bar{\mu}_z)$ transform correctly under E^* , the inversion operation in $D_{3h}(M)$.^{12,24} The transformation properties under the nuclear permutation operations in $D_{3h}(M)$ ^{12,24} impose symmetry relations between the expansion parameters $\mu_{kl\dots}^{\alpha(s)}$ ($\alpha=x, y, \text{ or } z$) in Eqs. (21)–(23); these relations have been derived analytically by means of MAPLE VI (Ref. 30) as described in Ref. 8.

We have already expressed the electronically averaged dipole moment in the electronic ground state of NH_3 in the MB representation [Eqs. (1)–(11) in conjunction with Table I] and we could now, in principle, obtain the dipole moment components $(\bar{\mu}_x, \bar{\mu}_y, \bar{\mu}_z)$ as analytical functions of the coordinates $\rho, \xi_1^l, \xi_2^l, \xi_3^l, \xi_{4a}^l, \text{ and } \xi_{4b}^l$ from the expression in Eq. (1). However, as detailed in Ref. 8, we have chosen instead the conceptually more complicated, but numerically simpler approach of obtaining, at each *ab initio* point, numerical values of $(\bar{\mu}_x, \bar{\mu}_y, \bar{\mu}_z)$ by carrying out, at the *ab initio* point in question, the coordinate transformation from the body-fixed axis system $x'y'z'$ used in the *ab initio* calculation (Sec. II A) to the xyz axis system. We then determine the values of the expansion parameters $\mu_{kl\dots}^{\alpha(s)}$ in Eqs. (21)–(23) by fitting Eq. (19) through the computed values of $(\bar{\mu}_x, \bar{\mu}_y, \bar{\mu}_z)$. The expansion parameters $\mu_{kl\dots}^{x(s)}$ and $\mu_{kl\dots}^{y(s)}$ in Eq. (21) are connected by symmetry relations since $(\bar{\mu}_x, \bar{\mu}_y)$ have E' symmetry in $D_{3h}(M)$, and so these two dipole moment components must be fitted together. The component $\bar{\mu}_z$, with A_2' symmetry, can be fitted separately. Taking Eq. (19) to sixth order, we fitted the $3 \times 14\,400$ *ab initio* data points using 174 parameters for the $\bar{\mu}_z$ component and 271 parameters for $(\bar{\mu}_x, \bar{\mu}_y)$. The rms deviations attained were 0.000 076 D and 0.0002 D, respectively.

IV. APPLICATIONS

A. Transition moments

With the dipole moment components $(\bar{\mu}_x, \bar{\mu}_y, \bar{\mu}_z)$ represented as given in Eq. (19) and the vibrational wave functions $|\Phi_{\text{vib}}^{(w)}\rangle$, $w=i$ or f , given by Eq. (12) for $J=0$, we compute the vibrational transition moments defined as

$$\mu_{fi} = \sqrt{\sum_{\alpha=x,y,z} |\langle \Phi_{\text{vib}}^{(f)} | \bar{\mu}_\alpha | \Phi_{\text{vib}}^{(i)} \rangle|^2} \quad (24)$$

for vibrational transitions in the electronic ground state of $^{14}\text{NH}_3$; the matrix elements required are generated by techniques described in Ref. 6 for matrix elements of the poten-

tial energy function. In calculating the vibrational wave functions, we use the *ab initio* potential energy surface CBS**–5 (Sec. III C) and a basis set with $P_{\text{max}}=14$ [Eq. (16)]. With this basis set, the $J=0$ matrix blocks corresponding to A and E symmetries in the group $D_{3h}(M)$ have the dimensions $N(A)=1455$ and $N(E)=2571$, respectively.

The values of the vibrational transition moments are, to a large extent, determined by the variation of the dipole moment components with the vibrational coordinates. By comparing our theoretical values for the vibrational transition moments to experimental values and other theoretical values available in the literature^{10,22,23,31–41} for $^{14}\text{NH}_3$, we can assess the quality of the ATZfc dipole moment surface. We make this comparison in Tables II and III. In these tables, the vibrational states are labeled such that a superscript + indicates the lower (symmetric) inversion component; the upper (antisymmetric) component is indicated by a superscript –. The symmetric and antisymmetric components of the vibrational ground state are labeled 0^+ and 0^- , respectively. In addition to the transition moment values obtained theoretically in the present work, Tables II and III give the available experimental values and the results of two other theoretical calculations by Marquardt *et al.*²² and Pracna *et al.*,³⁹ respectively. These latter results are analogous to ours in that they are pure *ab initio* predictions made without fitting to experiment. The work of Pracna *et al.*³⁹ also contains the results of such fittings, but we present here their “potential function I” results, obtained directly from *ab initio* data.

Our results agree very satisfactorily with the experimental transition moment values; the over-all agreement is better than that obtained in the two other theoretical calculations^{22,39} considered here. The most remarkable agreement is found for the fundamental transitions in Table II and for transitions to excited inversion states. The inversion motion in NH_3 involves tunneling between two equivalent minima on the potential energy surface and cannot be reasonably modeled by the motion of a one-dimensional harmonic oscillator. It is gratifying that, as shown in Tables II and III, our theoretical model describes well the intensities of transitions involving changes in the excitation of this complex motion, at least at low and moderate excitation. The transition moment results suggest that the ATZfc *ab initio* dipole moment surface (Sec. II A) is the most accurate dipole moment surface currently available for NH_3 .

B. Intensity simulations

As discussed in Sec. I, it is desirable to be able to simulate molecular spectra (i.e., to compute transition wave numbers and intensities) in order to assist their detection and subsequent first-principles assignment. In the present section, we report such simulations for $^{14}\text{NH}_3$ absorption bands starting in the lowest vibrational states 0^\pm and ending in the states $2\nu_2, \nu_4, \nu_1, \nu_3, \text{ and } 2\nu_4$. The simulated spectra are drawn as stick diagrams where the height of the stick representing a line is the integrated absorption coefficient from Eq. (18). The line strengths entering into this equation are computed from Eq. (21) of Ref. 8 with the spin statistical weight factors g_{ns} from Table 2 of Ref. 8. The simulations are made

TABLE II. Band centers ν_{fi} and vibrational transition moments μ_{fi} for ¹⁴NH₃: Transitions originating in the vibrational ground state.

States		ν_{fi} (cm ⁻¹)		μ_{fi} (D)			
f	i	Expt. ^a	Obs.	Reference ^b	Reference 39 ^c	Reference 22	Present work
0 ⁻	0 ⁺	0.79	1.471 93(1) ^d	31	1.536	1.574	1.4564
ν_2^+	0 ⁻	931.64	0.248(7)	32	0.269	0.2183	0.2445
ν_2^-	0 ⁺	968.12	0.236(4)	32	0.258	0.2075	0.2347
$2\nu_2^+$	0 ⁻	1596.68	0.020 36(25)	34	0.027	0.0091	0.0202
$2\nu_2^-$	0 ⁺	1882.18	0.003 256(35)	34	0.007	0.0261	0.0026
$3\nu_2^+$	0 ⁻	2383.36	0.004 96(13)	33	0.004	0.0261	0.0054
$3\nu_2^-$	0 ⁺	2895.51	0.002 856(40)	33	0.003	0.0155	0.0027
$4\nu_2^+$	0 ⁻	3461					0.0020
$4\nu_2^-$	0 ⁺	4055					0.0009
ν_1^+	0 ⁻	3335.23	0.026 2(1)	10		0.0366	0.0269
ν_1^-	0 ⁺	3337.08	0.026 2(1)	10		0.0366	0.0270
$(\nu_1 + \nu_2)^+$	0 ⁻	4293.72	0.0079	35		0.0067	0.0087
$(\nu_1 + \nu_2)^-$	0 ⁺	4320.06	0.007 9	35		0.0066	0.0083
ν_3^+	0 ⁺	3443.68	0.018 2(1)	10		0.0915	0.0181
ν_3^-	0 ⁻	3443.20	0.018 2(1)	10		0.0915	0.0180
$(\nu_2 + \nu_3)^+$	0 ⁺	4416.91	0.020 6	35		0.0128	0.0246
$(\nu_2 + \nu_3)^-$	0 ⁻	4434.61	0.020 6	35		0.0127	0.0244
ν_4^+	0 ⁺	1626.28	0.084 08(34)	34		0.0839	0.0828
ν_4^-	0 ⁻	1626.58	0.084 08(34)	34		0.0838	0.0827
$2\nu_4^{0,+}$	0 ⁻	3215.23	0.009 20(6) ^e	10			0.0073
$2\nu_4^{0,-}$	0 ⁺	3217.59	0.009 20(6) ^e	10			0.0074
$2\nu_4^{2,+}$	0 ⁺	3240.18	0.009 20(6) ^e	10			0.0091
$2\nu_4^{2,-}$	0 ⁻	3240.82	0.009 20(6) ^e	10			0.0090
$(\nu_2 + \nu_4)^+$	0 ⁺	2540.53	0.002 358(36)	33		0.0077	0.0091
$(\nu_2 + \nu_4)^-$	0 ⁻	2585.34	0.002 182(82)	33		0.0080	0.0094

^aDerived from the experimental data collected in Ref. 6.^bReference for the observed value given under the heading ‘‘Obs.’’^c*Ab initio* predictions, see text.^dExperimental uncertainties are given in parentheses (in units of the last digit quoted) where available.^eThe experimental value (Ref. 10) corresponds to the total $2\nu_4^{\pm}$ transition moments and should not be directly compared to the separate theoretical values for $2\nu_4^{0,\pm}$ and $2\nu_4^{2,\pm}$, respectively.

with the ATZfc *ab initio* dipole moment surface (Sec. II A) and the CBS**⁻⁵ potential energy surface (Sec. III C). We generate rovibrational wave functions with $J \leq 18$ and, in order to make the necessary variational calculations feasible, the size of the vibrational basis set is reduced to $P_{\max} = 8$ [Eq. (16)] relative to the $P_{\max} = 14$ basis set employed for calculating the vibrational transition moments in Sec. IV A. The largest matrix blocks obtained with the $P_{\max} = 8$ basis set are the E symmetry blocks at $J = 18$ with the dimension $N(E) = 9150$.

We compare our theoretical intensities with the results of two recent experimental studies of ¹⁴NH₃ absorption spectra: The $2\nu_2/\nu_4$ bands in the 5–7 μm region³⁴ and the $\nu_1/\nu_3/2\nu_4/4\nu_2$ bands near 3 μm .¹⁰ Both spectra have been recorded at room temperature. The experimental data (wave numbers and intensities) for the $2\nu_2/\nu_4$ bands, listed in the Appendix of Ref. 34, include 1203 rovibrational transitions between states with $J \leq 16$. The experimental data for the $2\nu_4/\nu_1/\nu_3$ bands⁴² are given in Appendix 1 of Ref. 10 and comprise 975 transitions between states with $J \leq 11$. We simulate spectra in the wave number regions 1300–2000 cm^{-1} (for the $2\nu_2/\nu_4$ bands) and 3000–3800 cm^{-1} (for the $2\nu_4/\nu_1/\nu_3$ bands) at $T = 295$ K. In computing the integrated absorption coefficient from Eq.

(18), we use the partition function value $Q = 1713.33$, which is obtained from the $J \leq 18$ term values calculated variationally below 6000 cm^{-1} , and the spin statistical weight factors for ¹⁴NH₃ from Table 2 of Ref. 8. We assign to each calculated eigenstate the vibrational quantum numbers V and the rotational quantum number K of the basis function with the largest contribution to the eigenfunction, i.e., with the largest value of $|C_{VK\tau_{\text{rot}}}^{(w)}|^2$ in Eq. (12). We discard transitions for which the calculated value of $I(f \leftarrow i) < 10^{-4} \text{ cm mol}^{-1}$. This threshold is much lower than the integrated absorption coefficient of the weakest observed line [a $2\nu_2$ band line with $I(f \leftarrow i) \approx 0.7 \text{ cm mol}^{-1}$] listed in Refs. 10 and 34.

In Figs. 2 and 3 we show simulations of the $2\nu_2$, ν_4 , $2\nu_4$, ν_1 , and ν_3 absorption bands of ¹⁴NH₃. The bands are artificially separated according to the assignment of the upper state. For example, in the 1300–2000 cm^{-1} wave number region (Fig. 2) we plot in separate displays the transitions to the ν_4 and $2\nu_2$ states, respectively. Each simulated band is compared to an ‘‘experimentally derived’’ stick spectrum drawn with experimental values for transition wave numbers and intensities;^{10,34} these transitions are also artificially separated according to the ‘‘experimental’’ assignment of the upper state. The experimentally derived spectra show only the

TABLE III. Band centers ν_{fi} and vibrational transition moments μ_{fi} for $^{14}\text{NH}_3$: Transitions originating in vibrationally excited states.

States		ν_{fi} (cm $^{-1}$)		μ_{fi} (D)			
f	i	Expt. ^a	Obs.	Reference ^b	Reference 39 ^c	Reference 22	Present work
ν_2^-	ν_2^+	35.69	1.244 8(23) ^d	36	1.305	1.355	1.2376
$2\nu_2^+$	ν_2^-	629.35			0.557	0.5084	0.5144
$2\nu_2^-$	ν_2^+	949.75	0.285 (10)	37	0.313	0.2698	0.2855
$3\nu_2^+$	ν_2^-	1416.03	0.073 7(16)	38	0.089	0.0288	0.0738
$3\nu_2^-$	ν_2^+	1963.08	0.000 81(11)	38	0.004	0.0416	0.0011
$4\nu_2^+$	ν_2^-	2494			0.012	0.0413	0.0088
$4\nu_2^-$	ν_2^+	3123			0.004	0.0184	0.0013
ν_1^+	ν_2^-	2367.90	0.004 0	38		0.0157	0.0002
ν_1^-	ν_2^+	2404.65	0.004 0	38		0.0159	0.0008
$(\nu_1 + \nu_2)^+$	ν_2^-	3326.39				0.0337	0.0244
$(\nu_1 + \nu_2)^-$	ν_2^+	3387.63				0.0312	0.0249
ν_3^+	ν_2^+	2511.25	0.022 86(29)	38		0.0080	0.0178
ν_3^-	ν_2^-	2475.87	0.022 86(29)	38		0.0080	0.0181
$(\nu_2 + \nu_3)^+$	ν_2^+	3484.48				0.0913	0.0320
$(\nu_2 + \nu_3)^-$	ν_2^-	3467.28				0.0907	0.0277
ν_4^+	ν_2^+	693.85				0.0022	0.0125
ν_4^-	ν_2^-	659.25				0.0022	0.0124
$2\nu_4^{+2,+}$	ν_2^+	2307.75	0.006 72(15)	38			0.0044
$2\nu_4^{+2,-}$	ν_2^-	2273.49	0.006 72(15)	38			0.0048
$2\nu_4^{0,+}$	ν_2^-	2247.90	0.000 85	38			0.0036
$2\nu_4^{0,-}$	ν_2^+	2285.16	0.000 85	38			0.0031
$(\nu_2 + \nu_4)^+$	ν_2^+	1608.10	0.088 8(12)	38		0.0867	0.0911
$(\nu_2 + \nu_4)^-$	ν_2^-	1618.01	0.084 3(27)	38		0.0856	0.0876
ν_1^-	ν_1^+	1.06	1.479 12(14)	23		1.599	1.4626
$2\nu_2^-$	$2\nu_2^+$	284.71	1.02(18)	40	0.995	1.047	0.9383
$3\nu_2^+$	$2\nu_2^-$	501.97	1.05(34)	40	0.898	0.9430	0.8876
$3\nu_2^-$	$2\nu_2^+$	1298.04			0.113	0.0830	0.1116
$4\nu_2^+$	$2\nu_2^-$	1580			0.050	0.0112	0.0512
$4\nu_2^-$	$2\nu_2^+$	2458			0.012	0.0454	0.0096
$3\nu_2^-$	$3\nu_2^+$	511.36			1.037	1.039	0.9671
$4\nu_2^+$	$3\nu_2^-$	566					0.9933
$4\nu_2^-$	$3\nu_2^+$	1671					0.0343
$4\nu_2^+$	$4\nu_2^-$	593			1.107	1.072	1.0199
ν_3^+	ν_3^-	0.31	1.509 4	23		1.626	1.4885
ν_4^+	ν_4^-	1.09	1.455 4(32)	41		1.574	1.4422

^aDerived from the experimental data collected in Ref. 6.^bReference for the observed value given under the heading Obs.^c*Ab initio* predictions, see text.^dExperimental uncertainties are given in parentheses (in units of the last digit quoted) where available.

transitions assigned in Refs. 10 and 34 and this explains why the experimental spectra generally contain less lines than the simulated ones. In the simulated and the experimentally derived stick spectra, the intensities are given as integrated absorption coefficients in cm mol $^{-1}$. The experimental values, originally^{10,34} given in cm $^{-2}$ atm $^{-1}$, were converted to cm mol $^{-1}$ at $T=295$ K. Note that the same absolute intensity scale is used for the two members of each theoretical/experimental spectrum pair.

It should be mentioned that in the wave number intervals 1300–2000 cm $^{-1}$ and 3000–3800 cm $^{-1}$, there are more vibrational bands than those assigned in Refs. 10 and 34. For example, the hot bands $(3\nu_2 - \nu_2)/(\nu_2 + \nu_4 - \nu_2)$ lie in the 5–7 μm region³⁸ and overlap with the $2\nu_2/\nu_4$ bands. This, of course, makes the experimental assignment more complicated. Also, the “theoretical assignment” based on the eigen-

vector coefficients $C_{VK\tau_{\text{rot}}}^{(w)}$ in Eq. (12) can differ from the “experimental assignment” in the event of strong accidental mixing of different basis functions in an eigenfunction. However, we do not expect such effects to be very important in the present study as we are not aiming at a line-by-line comparison of theory with experiment, but rather at a qualitative band-structure comparison. Therefore, we disregard possible misassignments and plot each simulated band separately as described above.

For the $2\nu_2/\nu_4$ band system shown in Fig. 2 there is significant similarity between the simulated and experimentally derived stick spectra, in particular, in the case of the ν_4 fundamental band, for which a large amount of experimental data (935 transitions) is available. Also for the $2\nu_4/\nu_1/\nu_3$ band system in Fig. 3 do the simulated fundamental bands ν_1 and ν_3 look highly similar to their experimental counterparts.

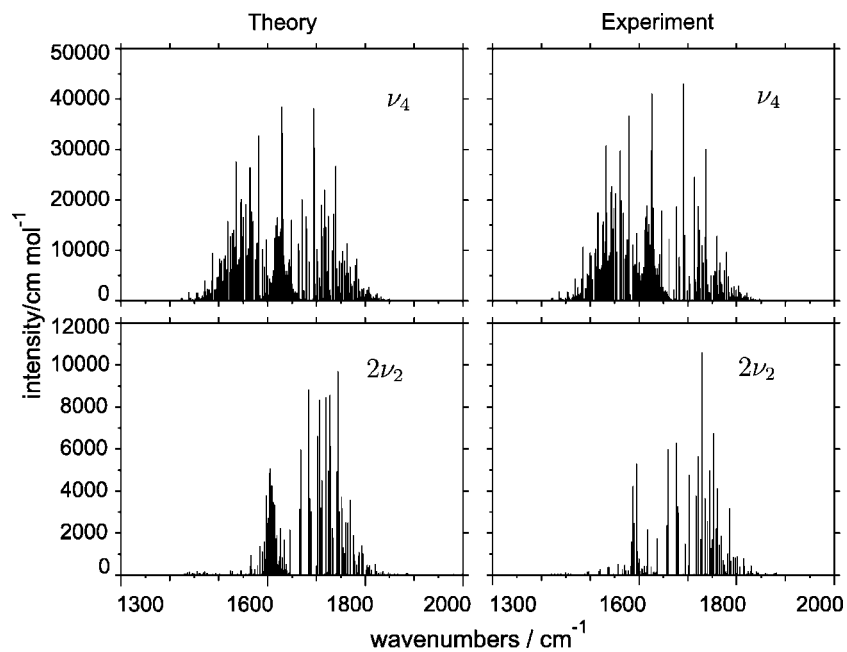


FIG. 2. Comparison of simulated and observed (Ref. 34) spectra near 5–7 μm : the ν_4 and $2\nu_2$ absorption bands of $^{14}\text{NH}_3$.

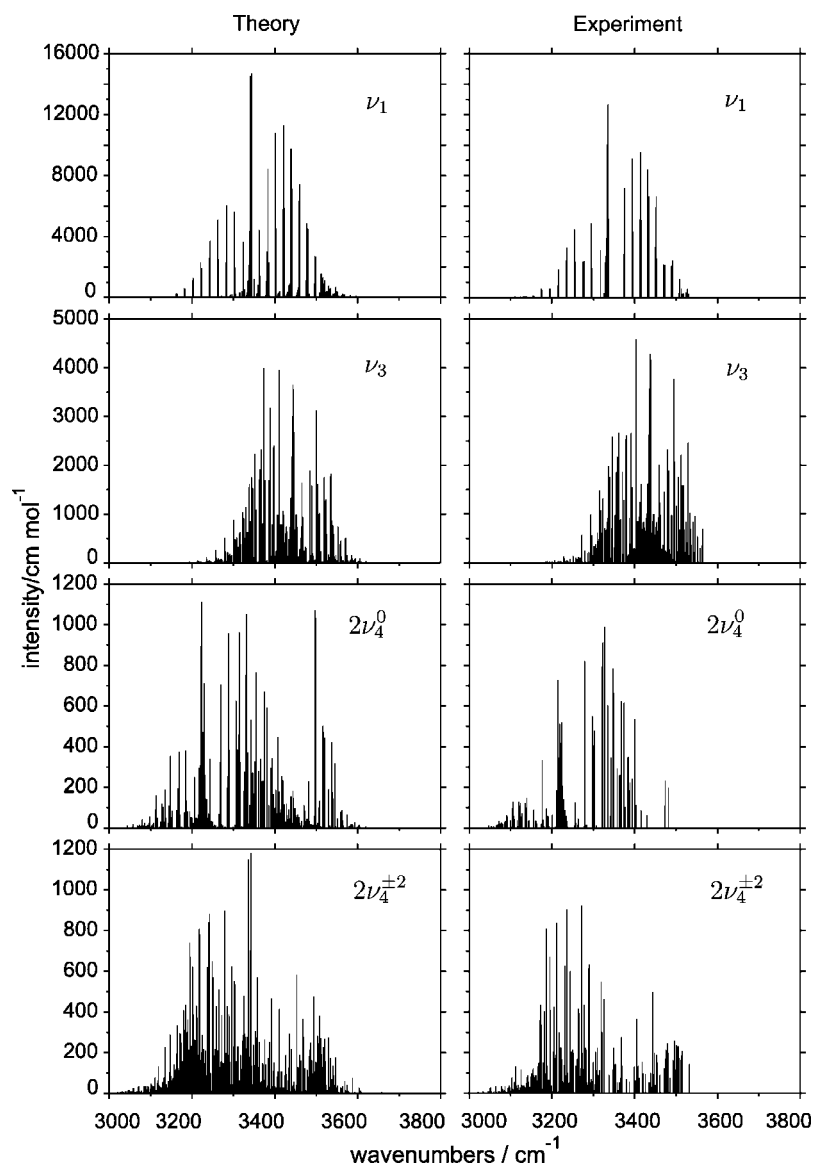


FIG. 3. Comparison of simulated and observed (Ref. 10) spectra near 3 μm : the ν_1 , ν_3 , $2\nu_4^0$, and $2\nu_4^{\pm 2}$ absorption bands of $^{14}\text{NH}_3$.

TABLE IV. Integrated absorption coefficients I (in $\text{cm}^{-2} \text{atm}^{-1}$) for the strongest rotation-vibration transitions in the ν_4 , $2\nu_2$, $2\nu_4$, ν_1 , and ν_3 bands of $^{14}\text{NH}_3$. In the transition labels, J_i , K_i , and Γ_i (J_f , K_f , Γ_f) are the J value, K value, and $D_{3h}(M)$ rotation-vibration symmetry, respectively, of the initial (final) state. The labels P , Q , R correspond to $\Delta J = J_f - J_i = -1, 0$, and 1 , respectively.

Band	$\Delta J(J_i)$	Γ_f	Γ_i	K_f	K_i	ν_{ij}^a	I (Obs.) ^b	I (Calc.) ^c
ν_4	$R(3)$	A_2'	A_2''	4	3	1691.737 32	1.750	1.551
$2\nu_2$	$R(6)$	A_2'	A_2''	6	6	1729.031 47	0.437	0.394
$2\nu_4^0$	$R(4)^d$	A_2''	A_2'	0	0	3323.524 43	0.037	0.042
$2\nu_4^{\pm 2}$	$R(3)$	A_2'	A_2''	4	3	3326.988 22	0.040	0.036
ν_1	$Q(3)$	A_2'	A_2''	3	3	3336.390 46	0.514	0.598
ν_3	$P(3)$	A_2'	A_2''	2	3	3403.383 91	0.186	0.160

^aExperimentally determined transition wave number (Refs. 10 and 34) in cm^{-1} .

^bExperimentally observed intensity (Refs. 10 and 34).

^cTheoretical intensity from the present work.

^dSecond-strongest line from the experimental $2\nu_4^0$ band transitions listed in Ref. 10 (see text).

The similarity is less pronounced for the weaker transitions to the overtone levels $2\nu_4$. It is obvious that for the $2\nu_4$ bands, the experimentally derived stick spectra contain significantly less lines than the simulations, and some of this dissimilarity may be due to the fact that not all $2\nu_4$ lines were assigned in Ref. 10, possibly because in the real spectrum, they overlap with stronger ν_1/ν_3 lines. The trend of the vibrational transition moments in Tables II and III is reflected in the line intensities: The vibrational transition moment of the ν_1 fundamental band is approximately twice as large as the ν_3 transition moment, and therefore the ν_1 band is approximately four times stronger than the ν_3 band.

In Table IV we compare theoretical and experimentally determined values for the integrated absorption coefficients of the strongest rotation-vibration transition in each of the five vibrational bands considered here. Also for these intensities of individual rotation-vibration lines, there is good agreement between theory and experiment. Each of the theoretical intensity values is relatively close to its experimentally observed counterpart. If we sort the lines in Table IV in order of increasing intensity, we obtain the sequence $2\nu_4^0 < 2\nu_4^{\pm 2} < \nu_3 < 2\nu_2 < \nu_1 < \nu_4$. Apart from the very small difference in intensity between the $|l_4|=0$ and 2 components of the $2\nu_4$ band, this sequence is correctly reproduced by the theoretical calculation and reflects the values of the vibrational transition moments in Tables II and III.

The largest disagreement between theory and experiment is obtained in the case of the $2\nu_4^0$ band. The strongest observed line in this band¹⁰ has the experimental assignment $R(4)$, $K_i=K_f=2$ [see the caption of Table IV for the explanation of the transition labels] and $I(\text{Obs.}) = 0.0402 \text{ cm}^{-2} \text{atm}^{-1}$. This line is theoretically predicted to be rather weak, $I(\text{Calc.}) = 0.015 \text{ cm}^{-2} \text{atm}^{-1}$, and we suspect that the high intensity of the observed line is caused by overlap with another unassigned line. Therefore, we compare in Table IV the observed and theoretical intensities for a more typical line, namely, that determined experimentally to be the second-strongest transition in the $2\nu_4^0$ band. Its experimental (and theoretical) assignment is $R(4)$, $K_i=K_f=0$. However, in the theoretical simulation it is the third-strongest $2\nu_4^0$ line. The two lines predicted to be slightly stronger are $Q(3)$, $K_i=K_f=3$ with $I(\text{Calc.}) = 0.045 \text{ cm}^{-2} \text{atm}^{-1}$ and $R(7)$, $K_i=K_f=2$ with $I(\text{Calc.}) = 0.044 \text{ cm}^{-2} \text{atm}^{-1}$. The theoretical $2\nu_4^{\pm 2}$

band also contains two extraneous lines stronger than the experimentally observed line $R(3)$, $K_i=3$, $K_f=4$ from Table IV. These lines are the two components ($+\leftarrow-$ and $-\leftarrow+$) of the line $Q(9)$, $K_i=9$, $K_f=7$ with $I(\text{Calc.}) = 0.048 \text{ cm}^{-2} \text{atm}^{-1}$ and $0.047 \text{ cm}^{-2} \text{atm}^{-1}$, respectively. Neither of the four extraneous $2\nu_4$ lines appears in the list of assigned lines in Ref. 10; we suspect that they overlap with stronger ν_1 or ν_3 lines.

In both of the wave number regions $1300\text{--}2000 \text{ cm}^{-1}$ [Fig. 2] and $3000\text{--}3800 \text{ cm}^{-1}$ [Fig. 3] considered here, the simulations of the weakest bands [$2\nu_2$ in the $1300\text{--}2000 \text{ cm}^{-1}$ region and $2\nu_4$ in the $3000\text{--}3800 \text{ cm}^{-1}$ region] show the largest discrepancies from the experimentally derived stick spectra. The most noticeable discrepancy is that, as mentioned above, the simulated spectra of weak bands contain significantly more lines than the experimentally derived ones. This indicates that in the weak bands, many lines were not assigned in the experimental studies of Refs. 10 and 34 even though their intensities appear significant in our simulations. Since in the experiment, all bands in a given wave number region are superimposed, it is plausible that many of these “extraneous” simulated weak-band lines overlap with strong-band lines in the observed spectrum, so that it is impossible to assign them.

C. Simplified intensity calculations

The simulations shown in Figs. 2 and 3 aim at high accuracy in each stage of the calculation. We now present the results of calculations where we degrade the accuracy of selected elements of the computational scheme in order to investigate how these elements influence the computed wave numbers and intensities. We focus on four elements of the calculation.

- The basis set. In the “standard” calculations producing Figs. 2 and 3, we used a basis set with $P_{\text{max}}=8$ [Eq. (16)].
- The expansion of the vibrational-coordinate dependent functions⁶ $G_{\alpha,\beta}$ in the kinetic energy operator. In the standard calculations, these expansions are truncated after fourth order in the linearized coordinates ξ_n^{ℓ} , $n = 1, 2, \dots, 5$.
- The expansion of the potential energy function V in

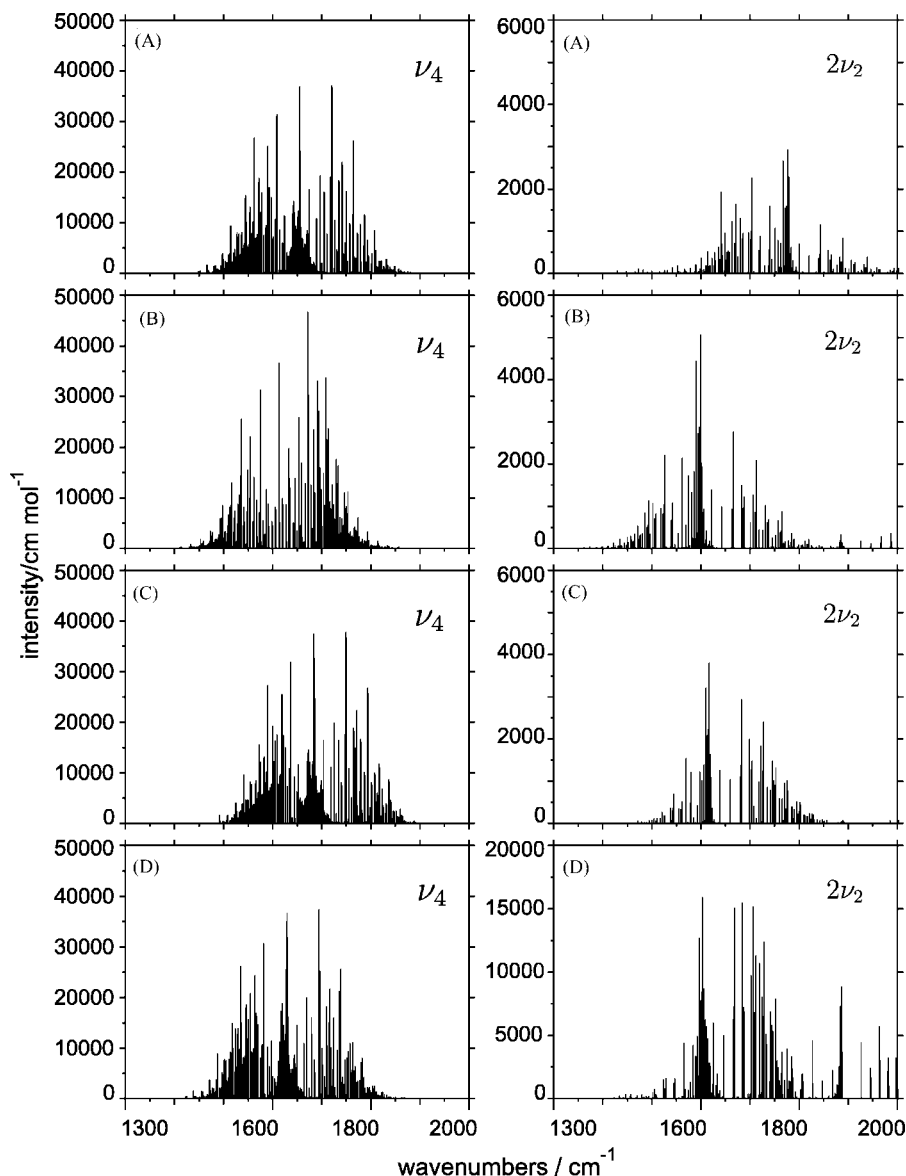


FIG. 4. The ν_4 and $2\nu_2$ bands of $^{14}\text{NH}_3$ simulated at $T=295$ K with (A) a reduced basis set, (B) a simplified kinetic-energy operator, (C) a simplified potential energy function, and (D) a simplified dipole moment representation (see text).

terms of the ξ_n^ℓ coordinates, taken to sixth order in the standard calculation.

- (d) The expansion of the dipole moment components $\bar{\mu}_\alpha$, $\alpha=x,y,z$ in the ξ_n^ℓ coordinates; these expansions are taken to sixth order in the standard calculation.

The simplest model for rovibrational intensities describes the rotation as that of a rigid symmetric rotor (taken to be the molecule at the equilibrium geometry) and the vibrational motion as that of uncoupled harmonic oscillators. That is, the wave function is a product of a rigid-rotor function and harmonic-oscillator eigenfunctions, while the electronically averaged dipole moment is represented as a first-order expansion in normal coordinates.^{12,24} This is known as the “doubly harmonic” approximation. As remarked in Sec. III A, it is inappropriate to model the inversion motion by a harmonic oscillator since the inversion involves the tunneling between two potential minima separated by a superable barrier. Therefore, in the “degraded” calculations, we maintain the numerically generated inversion basis functions also used in the standard calculations. These can be thought of as

rigid inverter wave functions.^{25,26} We also maintain in these test calculations the Morse-oscillator functions of Sec. III A as basis functions for the stretching motion, and so, in these calculations, we do not neglect the anharmonicity of the stretching motion.

We make test simulations of the ν_4 and $2\nu_2$ bands at $T=295$ K by degrading the calculations in the following manner.

- (A) *Basis set reduction*: We reduce the basis set to have $P_{\max}=2$ [Eq. (16)]; this is the smallest basis set capable of producing the upper states of the $\nu_4/2\nu_2$ transitions. The simulated spectra, shown in the “A” displays of Fig. 4, are drastically changed relative to the simulations in Fig. 2. Both the absolute intensities and the line positions undergo serious changes.
- (B) *Simplification of the kinetic energy operator*: To assess the importance of the kinetic energy operator for the quality of the spectrum simulations, we calculate intensities with the vibrational-coordinate-dependent functions $G_{\alpha,\beta}$ in the kinetic energy operator⁶ set equal to

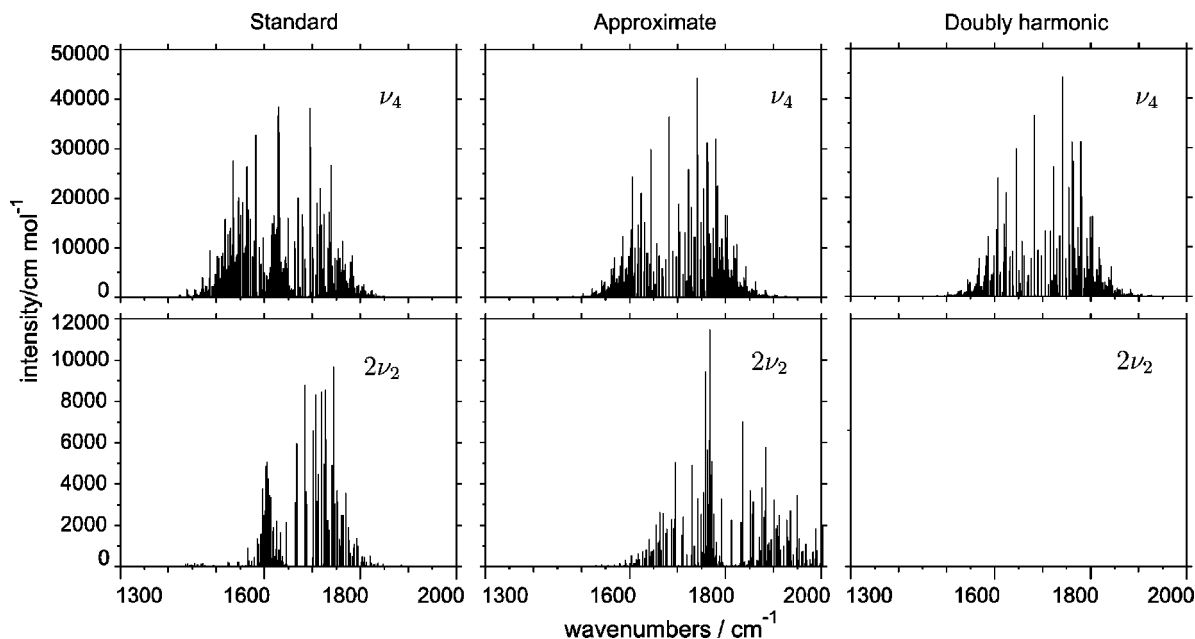


FIG. 5. The standard simulations of the $2\nu_2/\nu_4$ bands of $^{14}\text{NH}_3$ from Fig. 2 (labeled “Standard”), compared to simulations obtained in the approximation of making all four simplifications (A)–(D) simultaneously (labeled “Approximate”) and in the doubly harmonic approximation (labeled “Doubly harmonic”).

the zero-order term $G_{\alpha,\beta}^{(0)}(\rho) = G_{\alpha,\beta}(\rho, r_i^\ell = r_e, \alpha_i^\ell = \alpha_e)$ which depends on ρ only. $G_{\alpha,\beta}^{(0)}(\rho)$ is the value of $G_{\alpha,\beta}$ in the reference configuration. All other aspects of the calculation are kept in their standard form. The resulting simulated spectra are shown in the “B” displays of Fig. 4. The effect of the kinetic energy simplification is drastic: The simulated $2\nu_2$ band changes so much that it is hardly recognizable and the ν_4 band is also altered significantly from the standard simulation in Fig. 2.

- (C) *Simplification of the potential energy function:* We truncate the expression for the potential energy function after the second-order terms in the five linearized coordinates ξ_n^ℓ :

$$V = V^{(0)}(\rho) + \sum_k V_k^{(1)}(\rho) \xi_k^\ell + \sum_{kl} V_{kl}^{(2)}(\rho) \xi_k^\ell \xi_l^\ell \quad (25)$$

while keeping the basis set and the functions $G_{\alpha,\beta}$ in their standard forms. The effect of the potential energy truncation (shown in the “C” displays of Fig. 4) is noticeable but minor for the ν_4 band while very pronounced in the case of the $2\nu_2$ band.

- (D) *Simplification of the dipole moment expansion:* We simplify the analytical representation of the dipole moment components as much as possible by considering only the leading terms in Eq. (19):

$$\bar{\mu}_x = \mu_{4a}^x \xi_{4a}, \quad (26)$$

$$\bar{\mu}_y = \mu_{4a}^x \xi_{4b}, \quad (27)$$

$$\bar{\mu}_z = \mu_0^z \cos \rho; \quad (28)$$

all other parameters of the calculation are kept at their standard values. In this rather customary approxima-

tion, the ν_4 intensities derive solely from $\bar{\mu}_x$ and $\bar{\mu}_y$, whereas the intensity of the $2\nu_2$ band originates in $\bar{\mu}_z$. The simulated spectra are given in the “D” displays of Fig. 4. When we compare with the standard results in Fig. 2, there is no noticeable change in the structure of the ν_4 band. However, the $2\nu_2$ band, whose upper state is an excited inversion state, has completely lost its original structure.

When we compare Figs. 2 and 4, we see that for the ν_4 fundamental band, the degradation of the kinetic energy operator (B) has the largest influence on the intensity pattern. This is to be expected since the ν_4 band is a strong band that remains *allowed* (in the sense of Chapter 12 of Ref. 24) when we make the approximations (A), (C), (D) described above. The much weaker $2\nu_2$ band would be *forbidden* (in the sense of Chapter 12 of Ref. 24) if the vibrational wave functions were approximated by those of uncoupled harmonic oscillators and we use first-order expansions of the molecule-fixed molecular dipole moment components. This band is heavily influenced by all four approximations (A)–(D), and so, conversely, in order to obtain a correct description of it we must avoid these approximations.

As demonstrated in Fig. 4, the kinetic energy coupling between the different vibrational modes plays the most critical role in the determination of the rotational structure. An inaccurate description of this coupling fails to give correct intensity patterns for the *P*, *Q*, and *R* branches. The analogous potential energy coupling is also very important, especially for weak transitions that are forbidden in the doubly harmonic approximation. The intensities, and the wave number dependence on rotational excitation, of these transitions are crucially dependent on the anharmonic terms in the potential energy function. The electric anharmonicity also affects to some extent the rotational structure of transitions that

are forbidden in the doubly harmonic approximation, and moreover it has a pronounced effect on the vibrational intensity patterns.

In Fig. 5, we compare the standard simulations of the $2\nu_2/\nu_4$ bands (the corresponding displays, headed “Standard” in the figure, are repetitions of the simulations shown in Fig. 2) with the simulations obtained by making all four simplifications (A)–(D) simultaneously (labeled “Approximate”) and those obtained in the doubly harmonic approximation (labeled “Doubly harmonic”). The Approximate simulations differ from the Doubly harmonic ones in that in the Approximate calculation, the inversion motion is treated in the rigid inverter approximation,^{25,26} and the stretching motion is described by Morse-oscillator basis functions which account for anharmonicity. In addition, the Approximate dipole moment function is not strictly “electrically harmonic” because we express $\bar{\mu}_z$ in terms of the curvilinear coordinate ρ . Figure 5 shows that both in the doubly harmonic approximation and in the approximation defined by the four simplifications (A)–(D), the simulations are altered significantly relative to those obtained in the standard approximation, and the effect is much larger for the weak $2\nu_2$ band. Comparison of the simulated spectra under Approximate and Doubly harmonic shows that there are only minor changes in the appearance of the ν_4 band, in spite of the fact that there are no inversion splittings in the double harmonic approximation (these splittings are not visible on the scale of Fig. 5). There are drastic changes for the $2\nu_2$ band, of course, which carries no intensity in the doubly harmonic approximation.

V. SUMMARY AND CONCLUSION

We have presented extensive first-principles simulations of rotation-vibration spectra of ¹⁴NH₃. The calculations are carried out by means of recently developed computational methods for calculating rotation-vibration energies and intensities for isolated electronic states of XY₃ pyramidal molecules.^{6,8} By degrading the accuracy of selected elements of the calculations, and by doing calculations in the so-called doubly harmonic approximation, we have investigated the influence of customary approximations on the intensity values obtained. The result of these numerical experiments is an illustration of the properties of allowed and forbidden bands. The ν_4 band of ¹⁴NH₃ is allowed even in the crude approximation of rigid-rotor/harmonic-oscillator wave functions and an electrically harmonic dipole moment function. Therefore, this band is strong and its intensities are relatively insensitive to improvements in the intensity calculation. As strikingly demonstrated in Fig. 5, the $2\nu_2$ band requires electrical anharmonicity (i.e., an expansion of the dipole moment at least to second order in the normal coordinates) to gain intensity. It is forbidden in the doubly harmonic approximation. Consequently it is much weaker than the ν_4 band, and its intensity pattern is crucially dependent on the level of theory in the nuclear-motion calculation.

As witnessed by the vibrational transition moments in Tables II and III, the simulated spectra in Figs. 2 and 3, and the line strengths of individual rotation-vibration transitions

in Table IV, the theoretical intensity results of the present work are generally in very satisfactory agreement with the experimentally measured intensity values available for the electronic ground state of ¹⁴NH₃. Not only do we predict vibrational transition moments that explain the relative intensities of the observed vibrational bands, we also compute absolute line-strength values for individual rotation-vibration lines in good agreement with experimental results. Consequently, we expect that our computational method, in conjunction with high-quality *ab initio* potential energy and dipole moment surfaces, can simulate rotation-vibration spectra of XY₃ pyramidal molecules prior to observation with sufficient accuracy to facilitate the observation and assignment of these spectra.

ACKNOWLEDGMENTS

The initial stages of this work were supported by the European Commission through Contract No. HPRN-CT-2000-00022 “Spectroscopy of Highly Excited Rovibrational States.” The work of P.J. is supported in part by the Deutsche Forschungsgemeinschaft and the Fonds der chemischen Industrie.

¹S. V. Shirin, O. L. Polyansky, N. F. Zobov, P. Barletta, and J. Tennyson, *J. Chem. Phys.* **118**, 2124 (2003).

²O. L. Polyansky, A. G. Császár, S. V. Shirin, N. F. Zobov, P. Barletta, J. Tennyson, D. W. Schwenke, and P. J. Knowles, *Science* **299**, 539 (2003).

³D. Papoušek and M. R. Aliev, *Molecular Vibrational-Rotational Spectra* (Elsevier, Amsterdam, 1982).

⁴H. Lin, W. Thiel, S. N. Yurchenko, M. Carvajal, and P. Jensen, *J. Chem. Phys.* **117**, 11265 (2002).

⁵S. N. Yurchenko, M. Carvajal, P. Jensen, F. Herregodts, and T. R. Huet, *Chem. Phys.* **290**, 59 (2003).

⁶S. N. Yurchenko, M. Carvajal, P. Jensen, H. Lin, J. J. Zheng, and W. Thiel, *Mol. Phys.* **103**, 359 (2005).

⁷S. N. Yurchenko, W. Thiel, S. Patchkovskii, and P. Jensen, *Phys. Chem. Chem. Phys.* **7**, 573 (2005).

⁸S. N. Yurchenko, M. Carvajal, W. Thiel, H. Lin, and P. Jensen, *Adv. Quant. Chem.* (in press).

⁹H. Lin, J. J. Zheng, S. N. Yurchenko, P. Jensen, and W. Thiel (unpublished).

¹⁰I. Kleiner, L. R. Brown, G. Tarrago, Q.-L. Kou, N. Picqué, G. Guelachvili, V. Dana, and J.-Y. Mandin, *J. Mol. Spectrosc.* **193**, 46 (1999).

¹¹J. T. Hougen, P. R. Bunker, and J. W. C. Johns, *J. Mol. Spectrosc.* **34**, 136 (1970).

¹²P. R. Bunker and P. Jensen, *Molecular Symmetry and Spectroscopy*, 2nd ed. (NRC Research Press, Ottawa, 1998).

¹³P. Jensen, G. Osmann, and I. N. Kozin, in *Vibration-Rotational Spectroscopy and Molecular Dynamics*, edited by D. Papoušek (World Scientific, Singapore, 1997).

¹⁴MOLPRO2000 is a package of *ab initio* programs written by H.-J. Werner and P. J. Knowles, with contributions from R. D. Amos, A. Bernhardsson, A. Berning *et al.*

¹⁵C. Hampel, K. Peterson, and H.-J. Werner, *Chem. Phys. Lett.* **190**, 1 (1992), and references therein. The program to compute the perturbative triples corrections has been developed by M. J. O. Deegan and P. J. Knowles, *ibid.* **227**, 321 (1994).

¹⁶G. D. Purvis and R. J. Bartlett, *J. Chem. Phys.* **76**, 1910 (1982).

¹⁷M. Urban, J. Noga, S. J. Cole, and R. J. Bartlett, *J. Chem. Phys.* **83**, 4041 (1985).

¹⁸K. Raghavachari, G. W. Trucks, J. A. Pople, and M. Head-Gordon, *Chem. Phys. Lett.* **157**, 479 (1989).

¹⁹T. H. Dunning, *J. Chem. Phys.* **90**, 1007 (1989).

²⁰D. E. Woon and T. H. Dunning, *J. Chem. Phys.* **98**, 1358 (1993).

²¹S.-G. He, J. J. Zheng, S.-M. Hu, H. Lin, Y. Ding, X.-H. Wang, and Q.-S. Zhu, *J. Chem. Phys.* **114**, 7018 (2001).

²²R. Marquardt, M. Quack, I. Thanopoulos, and D. Luckhaus, *J. Chem. Phys.* **119**, 10724 (2003).

- ²³M. D. Marshall, K. C. Izgi, and J. S. Muentner, *J. Chem. Phys.* **107**, 1037 (1997).
- ²⁴P. R. Bunker and P. Jensen, *Fundamentals of Molecular Symmetry* (IOP Publishing, Bristol, 2004).
- ²⁵D. Papoušek, J. M. R. Stone, and V. Špirko, *J. Mol. Spectrosc.* **48**, 17 (1973).
- ²⁶V. Špirko, *J. Mol. Spectrosc.* **101**, 30 (1983).
- ²⁷E. Anderson, Z. Bai, C. Bischof *et al.*, *LAPACK Users' Guide*, <http://www.netlib.org/lapack/>, Third Edition, 1999.
- ²⁸P. Jensen and V. Špirko, *J. Mol. Spectrosc.* **118**, 208 (1986).
- ²⁹P. Jensen, *J. Mol. Spectrosc.* **132**, 429 (1988).
- ³⁰M. B. Monagan, K. O. Geddes, K. M. Heal, G. Labahn, S. M. Vorkoetter, and J. McCarron, *Maple 6 Programming Guide*, Waterloo Maple, Toronto, 2000.
- ³¹K. Tanaka, H. Ito, and T. Tanaka, *J. Chem. Phys.* **87**, 1557 (1987).
- ³²T. Nakanaga, S. Kondo, and S. Saëki, *J. Mol. Spectrosc.* **112**, 39 (1985).
- ³³I. Kleiner, G. Tarrago, and L. R. Brown, *J. Mol. Spectrosc.* **173**, 120 (1995).
- ³⁴C. Cottaz, I. Kleiner, G. Tarrago *et al.*, *J. Mol. Spectrosc.* **203**, 285 (2000).
- ³⁵J. S. Margolis and Y. Y. Kwan, *J. Mol. Spectrosc.* **50**, 266 (1974).
- ³⁶Y. Ueda and J. Iwahori, *J. Mol. Spectrosc.* **116**, 191 (1986).
- ³⁷P. H. Beckwith, D. J. Danagher, and J. Reid, *J. Mol. Spectrosc.* **121**, 209 (1987).
- ³⁸C. Cottaz, G. Tarrago, I. Kleiner, and L. R. Brown, *J. Mol. Spectrosc.* **209**, 30 (2001).
- ³⁹P. Pracna, V. Špirko, and W. P. Kraemer, *J. Mol. Spectrosc.* **136**, 317 (1989).
- ⁴⁰M. Takami, H. Jones, and T. Oka, *J. Chem. Phys.* **70**, 3557 (1979).
- ⁴¹H. Sasada, Y. Hasegawa, T. Amano, and T. Shimizu, *J. Mol. Spectrosc.* **96**, 106 (1982).
- ⁴²Here, we only discuss the intensities of the vibrational transitions to the ν_1 , ν_3 , and $2\nu_4$ states; the amount of experimental data available for the $4\nu_2$ band is very limited.